

A novel splitter design for microfluidic biochips using centrifugal driving forces

Samuel I. En Lin

Received: 21 October 2009 / Accepted: 7 January 2010 / Published online: 29 January 2010
© Springer-Verlag 2010

Abstract Enzyme-linked immunosorbent assay (ELISA) is the most widely used immunoassay for the detection and quantification of biological agents (mainly proteins and polypeptides). One challenge in developing microfluidic devices for immunogenic and enzymatic assays is to split the fluid evenly into microchannels. To prevent uneven splitting, we propose a buffer-structure design, which holds the stream lines in the radial direction before they enter into bifurcation channels. To study the feasibility of this design, a three-dimensional numerical model, based on the Navier–Stoke equation, was constructed. Upon verification, it was successfully demonstrated that the proposed half-circle design can split flow evenly under the existence of Coriolis forces during operation.

Keywords CD-ELISA · Microfluidic · Splitter · ELISA

1 Introduction

Enzyme-linked immunosorbent assay (ELISA) is one of the most commonly used immunoassays that detects and quantifies chemical and biological molecules (antigens; mainly proteins and polypeptides). It is becoming more and more important in clinical diagnostics, food safety testing, and environmental monitoring. CD-ELISA aims to perform

the ELISA process on a compact-disk (i.e., CD) microfluidic platform. The concept is to utilize its unique microfluidic function, i.e., flow sequencing, to replace the stepwise procedures carried out in the conventional ELISA process. CD-ELISA is a self-contained microdevice that incorporates low-power microfluidic components and high-sensitivity immunomolecules and is capable of performing parallel and multiple tests with high precision. As a result, for many widely used ELISA-based systems, a user-friendly CD-ELISA chip would be highly desirable. The key issues involved in the development of microfluidic CD-ELISA devices include microfabrication technology, microfluidic components, surface modification and immobilization, and biomolecule detection methods; as a result there is a wide research area for future investigations.

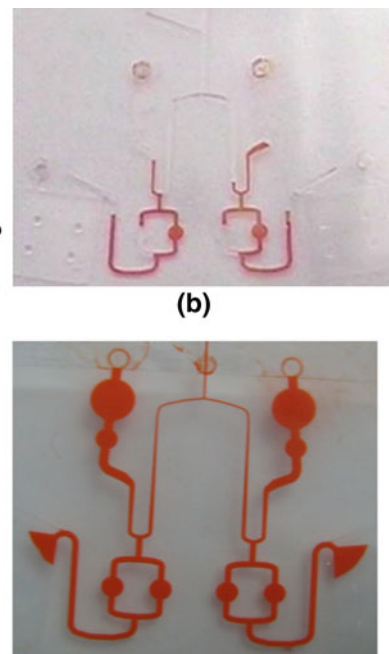
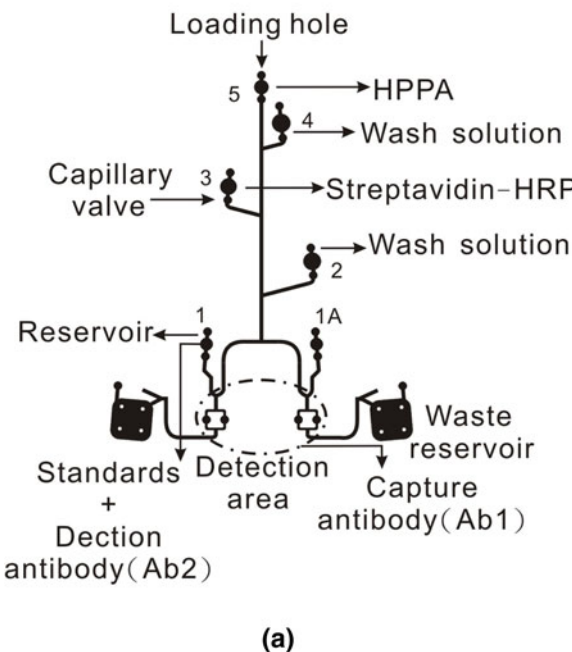
Centrifugal fluidic platform technology was first developed in 1969 (Anderson 1969), and this concept has since been extensively studied (Scott and Burtis 1973; Klumpp 1977; Bonte et al. 1977; Henry et al. 1978). It is beneficial in many analytical situations due to its versatility in handling a wide variety of sample types, ability to gate the flow of liquids (valving), simple rotational motor requirements, economic and simple fabrication methods, large range of attainable flow rates, and easy adaptation to existing optical detection methods. Most analytical functions required for a lab-on-a-disk including metering, dilution, mixing, calibration, and separation have all been demonstrated in the laboratory. Moreover, the possibility of maintaining simultaneous and identical flow rates, to perform identical volume additions, establish identical incubation times, mixing dynamics, and detection in a multitude of parallel assay elements makes the CD an attractive platform for multiple parallel assays. Substrates, conjugates, wash buffers, primary antibodies, blocking proteins, and antigen solutions can be preloaded into

S. I. E. Lin (✉)
Department of Power Mechanical Engineering,
National Formosa University, Hu-Wei Town,
Yunlin, Taiwan, ROC
e-mail: samlin7@ms41.hinet.net

corresponding reservoirs prior to testing. Centrifugal and capillary forces are used to control the flow sequence of different solutions involved in the ELISA process (Silva et al. 2009; Brenner et al. 2005). A computer controls the rotational speed of the disk to achieve proper flow sequencing and incubation.

To increase the sample capacity of the CD-ELISA chip and further reduce cost, a design incorporating splitters of ELISA microdevices is needed for multi-sample assay analysis. The concept of a splitter is commonly employed in microfluidic platforms to distribute the fluid flow. In a 5-reservoir ELISA process, only the composition of the antigen is different, whereas all other reagents used in the assay have the same composition. Therefore, one splitter is designed for reservoirs, 1 and 1A (see Fig. 1a), each of which is used for the loading of two individual samples (antigens). The splitters for the detection area shown in Fig. 1a are designed for sample duplication. This ‘model chip’ design allows for comparison and testing of splitters on a single CD. Ideally, the splitters in this design would increase the 12 sets on a CD-ELISA chip, providing the capability to analyze 24 samples in duplicate—a 48-sample assay analysis. However, the Coriolis force vector resulting from the disk rotation can bias the flow rate and thus cause uneven flow volume into the microchannels (Fig. 1b) (Brenner et al. 2005). In this study, we propose a splitter structure which can overcome this unbalanced flow. Both theoretical and experimental works were carried out, with experimental data showing a promising feature in our new design.

Fig. 1 a Schematics of a CD-ELISA design with one assay, b the image shows the uneven splitting condition after CD rotation, c the image shows the experimental work of the proposed half-circle structure which provides a better splitting ratio



2 Theory

Fluid mechanics deals with the study of gases and liquids either in motion (fluid dynamics) or at rest (fluid statics). When studying liquid flows, it is often safe to assume that the material’s density is constant or near constant. We therefore approach this problem with an incompressible fluid flow. Using the incompressible Navier–Stokes equation, we solve the transient models of incompressible fluid dynamics. A schematic drawing for the present problem is illustrated in Fig. 2a, b. Before splitting, there is a loading hole where fluid is loaded. After splitting, we have two reservoirs which simulate the detection areas. The generalized equations in terms of transport properties and velocity gradients are

$$\rho \left[\frac{\partial \mathbf{u}}{\partial t} + (\mathbf{u} \cdot \nabla) \mathbf{u} \right] = \mathbf{F} - \nabla p + \mu \nabla^2 \mathbf{u} \quad (1)$$

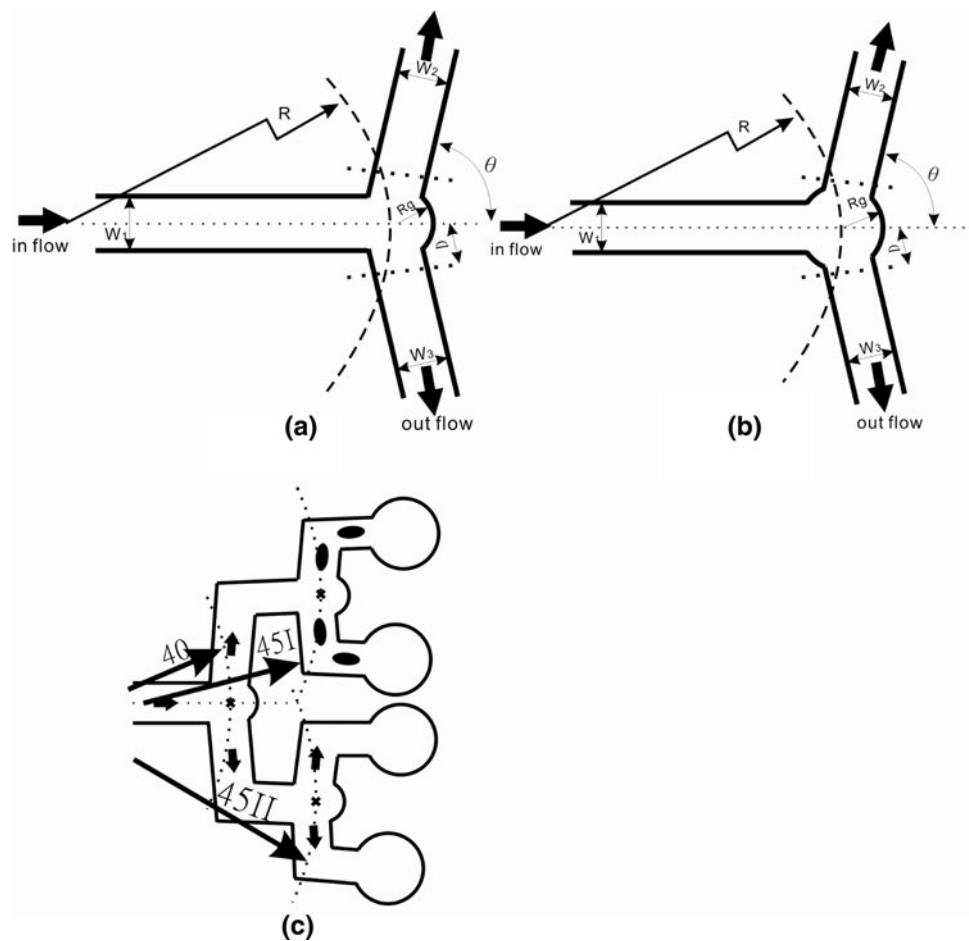
$$\nabla \cdot \mathbf{u} = 0, \quad (2)$$

where \mathbf{u} , p , ρ , and μ are the velocity vector, pressure, density, and dynamic viscosity, respectively. Also \mathbf{F} denotes the volume force term which includes the gravitational force, the centrifugal force vectors, and the Coriolis force. Thus, the volume force term can be written as

$$\mathbf{F} = \rho \mathbf{g} + \mathbf{F}_{ce} + \mathbf{F}_{co} = \rho \left(\mathbf{g} + |\boldsymbol{\omega}|^2 \mathbf{r} - 2\boldsymbol{\omega} \times \mathbf{u} \right), \quad (3)$$

where \mathbf{g} is the gravity vector, \mathbf{r} is the radial position vector, and $\boldsymbol{\omega}$ is the angular velocity vector. In Cartesian

Fig. 2 The design parameters used on the splitter: **a** the splitter has a half-circular buffer structure; **b** the splitter has a circular buffer structure; **c** the cascaded splitters 40, 45I, and 45 II. The numeric values represent the distance (mm) away from the center of CD. Here, we use a half-circular buffer structure, as illustrated



coordinates, we express the volume force using three direction components, $\mathbf{F} = (\mathbf{F}_x, \mathbf{F}_y, \mathbf{F}_z)$. We further apply a flow rate \mathbf{u} , such that

$$\mathbf{u} = u_x \mathbf{i} + u_y \mathbf{j} + u_z \mathbf{k}. \quad (4)$$

Since the disk is rotating with the surface facing upwards, the angular velocity and gravity are expressed as

$$\boldsymbol{\omega} = \omega_z \mathbf{k}, \quad g = g_z \mathbf{k}, \quad (5)$$

respectively. The no-slip boundary condition (i.e., $\mathbf{u} = 0$) is used on the boundary (i.e., around the square cross section of the channel) as a first approximation. Since the driving force comes from the centrifugal force, we do not need any initial condition in Eq. 1. For a first approximation, the two-phase flow (i.e., moving boundary between water and air) is not considered in the present model. The fluid properties and three-dimensional model geometry are listed in Table 1.

3 Experimental setup

Polymethyl methacrylate (PMMA) CD-like plates were used in the experimental study. Microfluidic channels were

Table 1 The working parameters used in the computation of Navier–Stoke equation

Parameters	Values
Density	997 kg/m ³
Dynamic viscosity	8.91×10^{-4} N/m ²
Radius	40 mm
Rotation (rpm)	1000
Channel width and height (mm)	0.3×0.3
Half-circle structure, radius (mm)	0.3
Full-circle structure, radius (mm)	0.3

machined using a high-speed (50K RPM) Computer Numerical Control (CNC) on the flat PMMA channel surface (cf. Fig. 1c). The schematic drawing of the channel geometry is shown in Fig. 2a–c. There are six groups implemented in this experiment and their corresponding channel geometries are listed in Table 2. The channel width and depth is designed to be 300 μm , which is about the same order used in other work (Lu et al. 2007; Brenner et al. 2005). The six groups were chosen in order to study the effects of: (1) splitter design with a half-circle buffer

Table 2 Six groups were studied in this experiment in order to investigate the effects of buffer structure and position stability

Parameters\groups	#1	#2	#3	#4	#5	#6
W ₁ (mm)	0.3	0.3	0.3	0.3	0.3	0.3
W ₂ (mm)	0.3	0.3	0.3	0.3	0.3	0.3
W ₃ (mm)	0.3	0.3	0.3	0.3	0.3	0.3
R _g (mm) half	0.3	0.4	0.6			
R _g (mm) full				0.3	0.4	0.6
θ (°)	85	85	85	85	85	85
R (mm)	40	45I	45II	40	45I	45II

structure, (2) splitter design with a full-circle buffer structure, (3) a cascaded splitter design which has a different distance away from center point of the CD. The first two items were used to study the effects of a buffered structure on the splitting ratios, whereas the third was utilized to investigate the stability of the splitting capability. Since Coriolis force has less influence at mild rotational speed (Brenner et al. 2005), we therefore adopt 1000 rpm in the experimental work. During this study, in order to eliminate effects other than the Coriolis force, the inflow channels (before each splitter in the PMMA CD test bench) were aligned in a radial direction. The other parameters, such as bifurcation angle, channel roughness, and channel width, have been discussed in a separate study (Lu et al. 2007; Lin and Chen 2008). De-ionized (DI) water was added by using a volume control pipette and was applied in the loading area each time. There were 40 runs in each group and measurements on the splitting ratios were carried out accordingly. The splitting ratios are the fluid volume measurements in the detection area, captured by a CCD image. The motor was connected to an encoder to trigger a strobe (Monarch, DA 115/Nova Strobe) for synchronized imaging. Dyed fluid totally covering the detection area was recorded as 100%. The loading area was designed to be smaller than the detection area so that there

would not be any issues of overflowing during experiments.

A PLGA solution was prepared by dissolving 2 g of PLGA in 10 g of acetonitrile. A thin layer of PLGA film was spin-coated onto a blank PMMA cover at 1500 rpm for 1 min using a spin coater. The spin-coated cover was then placed in a vacuum oven overnight for drying. Before bonding, the PMMA cover was aligned with the microfluidic chip and the whole assembly was placed inside the pressure chamber at 40°C. The CO₂ pressure was introduced and increased to 1.5 MPa for 1 h. The bonding took 1 h, followed by a slow pressure release of CO₂ gas at 0.3 MPa/min to avoid foaming.

The CD-based microfluidic platform with a programmable stepping motor was also utilized in this experiment. The computer-controlled spindle can run at a constant revolution for a specified time period and move to the next specified revolution. All channels were cleaned and dried using an antistatic air-gun each time in order to have uniform surface quality across all experiments. The channel surface quality can affect the flow velocity and therefore plays an important role in the splitter design. In this study, we employed a white light interferometer (MSA-400 from Polytec GmbH, Germany) with a 50× objective lens to measure the channel surface quality.

4 Results and discussions

Instead of using a protein solution, we applied DI water colored with 5.0 wt% food dye for verification purposes. The CD bench test was rotating constantly at 1000 rpm for computational purposes. The DI water properties and other working parameters are listed in Table 1 and were used in the computer simulation. The stream line profiles for different splitter designs are shown in Figs. 3, 4, and 5. The velocity profiles across the microfluidic cross section are depicted in Figs. 6, 7, and 8 for all case studies.

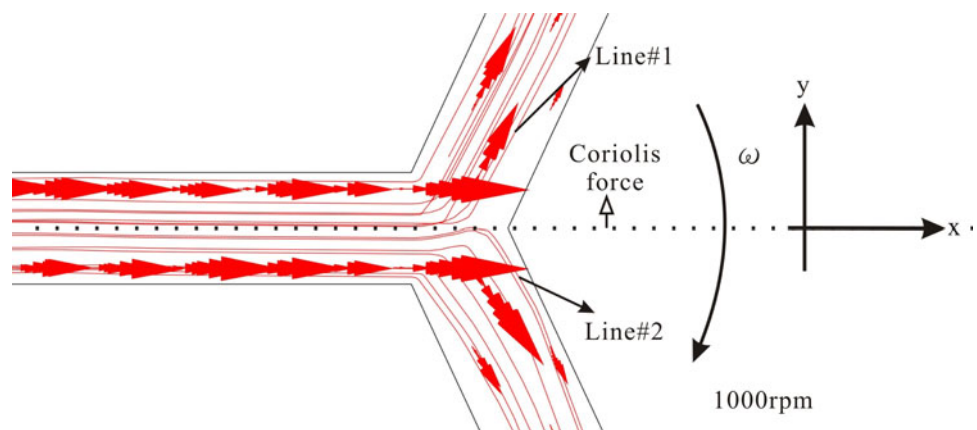
Fig. 3 Stream line profiles of the conventional splitter obtained from computational modeling. The stream lines clearly experience drag due to the Coriolis force near the tip of the bifurcation point. The bifurcation angle is set to be 65°

Fig. 4 Stream line profiles of full-circle structure obtained from computational modeling. The stream lines are pushed by the Coriolis force and deviate from the centerline. The bifurcation angle is set to be 65°

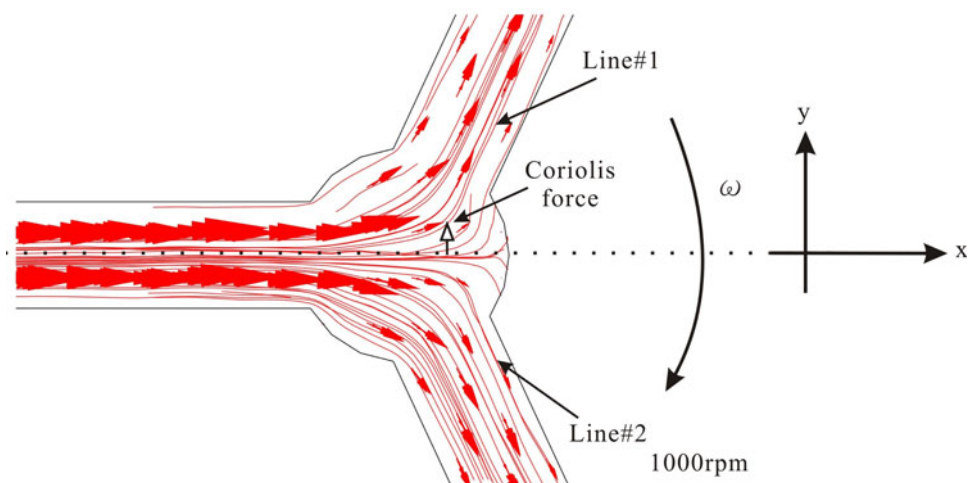


Fig. 5 Stream line profiles of the half-circle structure obtained from computational modeling. The stream lines remain unchanged near the centerline until they hit the bifurcation region. The bifurcation angle is set to be 65°

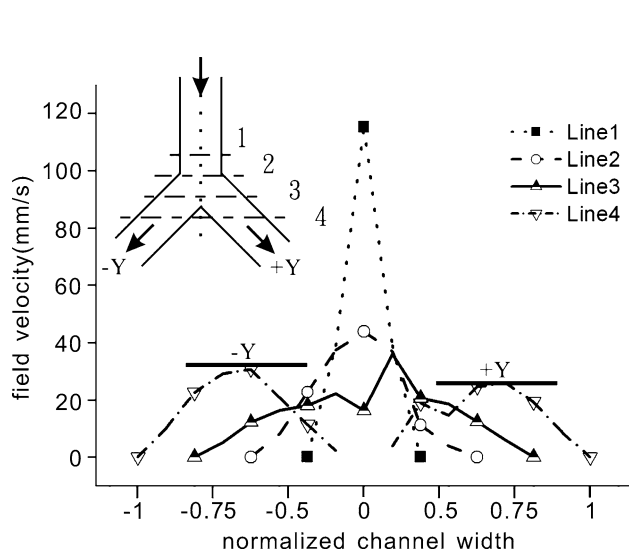
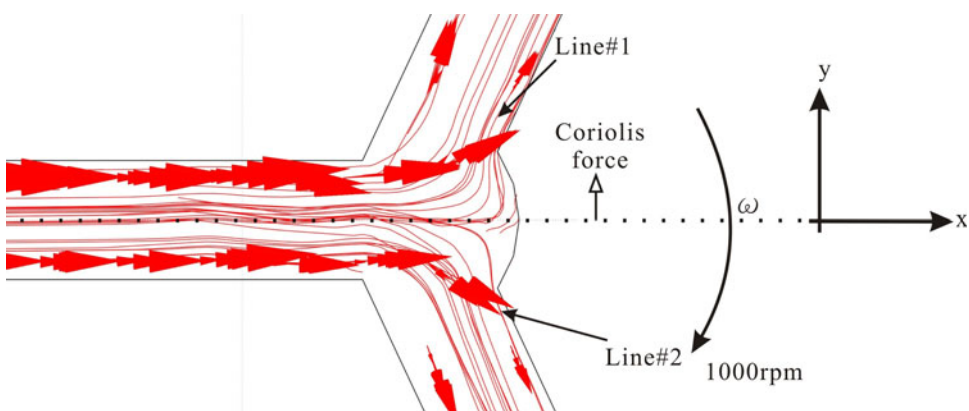


Fig. 6 The velocity profiles of a conventional splitter computed at the post-splitter region. The velocity data were adopted across the channel cross section from lines #1 to #4 as indicated in the upper-left figure. The normalized channel width -1 represents the left boundary of the line #4, whereas $+1$ indicates the right boundary of the line #4

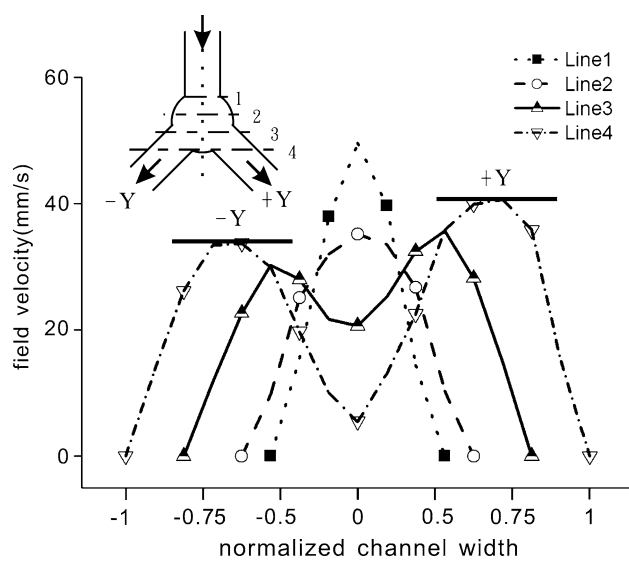


Fig. 7 The velocity profiles of the full-circle structure computed at the post-splitter region. The velocity data were adopted across the channel cross section from lines #1 to #4 as indicated in the upper-left figure. The normalized channel width -1 represents the left boundary of the line #4, whereas $+1$ indicates the right boundary of the line #4

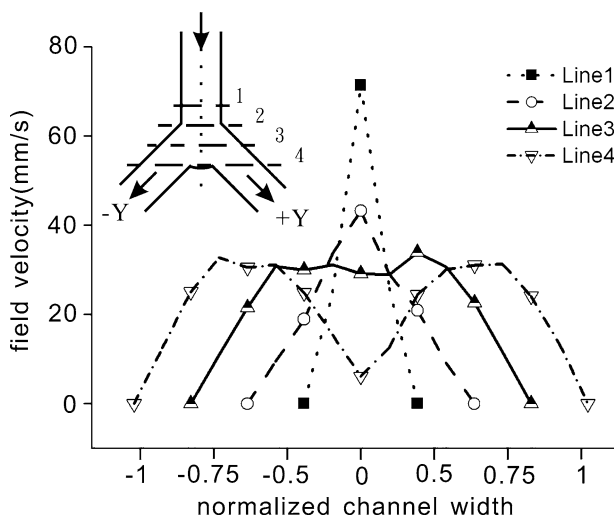


Fig. 8 The velocity profiles of the half-circle structure computed at the post-splitter region. The velocity data were adopted across the channel cross section from lines #1 to #4 as indicated in the upper-left figure. The normalized channel width -1 represents the left boundary of the line #4, whereas $+1$ indicates the right boundary of the line #4

4.1 Computational results

4.1.1 Stream line profiles

Streamlines are a family of curves that are instantaneously tangent to the velocity vector of the flow. These show the direction in which a fluid element will travel at any point with respect to time. The conventional splitter has no buffer zone. The streamline form two branches on the splitter region and they are not symmetric with respect to the center axis due to Coriolis forces (Fig. 3). Line #1 deviates from the center prior to #2 due to the effects of the Coriolis force (represented by an arrow in Fig. 3). Line #2 was dragged toward the $+Y$ -direction (due to the Coriolis force) close to the tip of the apex region. However, it flows into the $-Y$ channel at the last minute due to the geometric separation. It results in an unbalanced flow rate over the splitter, as observed in the experimental work (see Fig. 1b). The buffer zone design was therefore proposed to improve this uneven flow splitting.

Figure 4 shows the streamline profiles of the full-circle splitter design. The streamline #1 was clearly pushed by the Coriolis force (denoted by an arrow), whereas the line #2 remains much straighter toward the end of circle buffer region. Unlike Fig. 3, no streamlines were dragged over the centerline or turn to the $+Y$ -direction before flowing into the $-Y$ channel. This indicates that more flow will go into the $+Y$ channel as we will discuss in the following section.

The streamlines' profiles of the half-circle structure are presented in Fig. 5 at 1000 rpm clockwise rotation, the same operation mode as we used in Figs. 3 and 4. The streamline

#1 and #2 exhibit more symmetric conditions as compared with the other two structures. The rest of the stream lines remain symmetric in this design as we observed in Fig. 5. This structure thus may provide the possibility of evenly splitting during operation. The half-circle design keeps the stream lines in the radial direction and withstands the Coriolis force before the flow branches off.

4.1.2 Velocity profiles

The stream lines provide the insight of how the Coriolis force affects the flow before it branches into channel. The velocity profiles directly indicate the splitting ratio between the two channels. The field velocity profiles, across the channel section, at various positions are shown in Figs. 6–8. The working parameters are listed in Table 1 and the CD rotates at 1000 rpm.

It is clearly shown that the velocity profile is symmetric before the flow enters the bifurcation region in the conventional splitter (Fig. 6, line #1). As the flow propagates toward the bifurcation region (i.e., line #3 in Fig. 6), the Coriolis force comes into effect and biases the velocity profile. After the flow enters the branches, the peak velocity shows a difference in $-Y$ and $+Y$ directions (i.e., line #4 in Fig. 6). The integration of the velocity profile across the channel width concludes the splitting ratio and is $+Y/-Y = 1/1.08$. This profile difference (line #4) results from Coriolis forces and thus causes uneven flow into the branches. The greater the rotational speed, the more uneven the flow splitting.

The velocity profile changes under different splitter structures. Figure 7 shows the profile of a full-circle structure at various positions. The flow profile is perfectly symmetric before it enters the bifurcation region (i.e., line #1 in Fig. 7). Once this flow enters the expanded circular region, the peak velocity reduces (i.e., line #2 in Fig. 7), but still remains symmetric. Before the flow reaches the separation region, the Coriolis force makes the velocity become slightly asymmetric at line #3. The significant peak difference (line #4) occurs in the branch region and thus yields the uneven splitting ratio $+Y/-Y = 1/0.89$. More flow rate was attracted into the $+Y$ channel due to the effects of the Coriolis force in the expanded circular region.

The field velocity profiles of the improved half-circle structure are shown in Fig. 8. The velocity profiles remain symmetric over the bifurcation region (i.e., lines #1 to 4 in Fig. 8). The effects of the Coriolis force have less impact on the half-circular design and thus provide a better splitting ratio $+Y/-Y = 1/0.99$. The proposed splitter design, which utilizes the buffer zone concept, does improve the splitting ratio in comparison with the conventional structure in this simulation. All the velocity profiles presented in

the analysis are adopted from the half-depth region of the fluidic channel. The four boundaries on the square cross section are slip-free. The simulations were verified by experiment, as is described in the following section.

4.2 Experiments

There are six groups in the splitter configuration (see Table 2) and they are all integrated into one PMMA CD. The initial CD rotated at 100 rpm for 5 min, and then increased to 1000 rpm so the flow can pass the designed valves and reach detection areas (Fig. 1c). This will result in all the DI water in the reservoir passing to the valves with no residual water left in the channel. Detailed preparation and experimental setups have been discussed in Sect. 3.

4.2.1 Effects of cascaded splitters

In clinical applications, the splitter must have the same splitting ratio regardless of the position. We therefore investigated the splitting stability of the proposed splitting structure. For the full-circle design, the splitting ratios at the cascaded splitter are shown in Fig. 9 (with $R_g = 0.3$ mm). They were 1.197, 1.212, and 1.353 as measured at radial positions 40, 45I, and 45II, respectively. The uneven splitting ratio becomes worse as we observed in the cascaded radial position. On the other hand, the splitting ratios of the half-circle design exhibited much better results. For positions 40, 45I, and 45II, they were 1.0683, 1.01901, and 1.030, respectively (see Fig. 9). The data from the half-circle design yielded very promising results on the current channel geometry (see Fig. 1c for illustration).

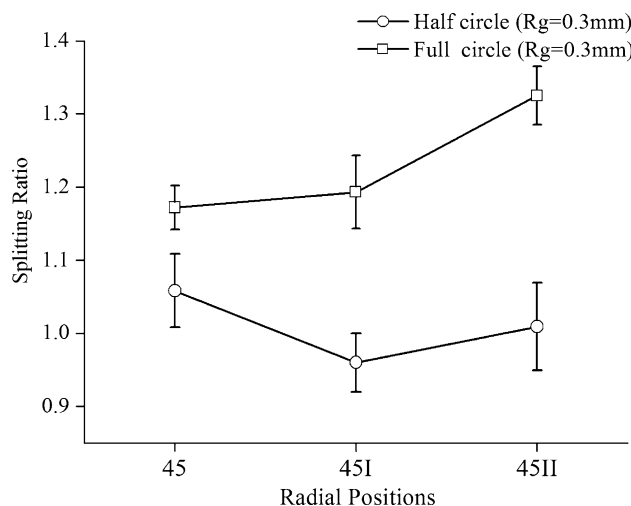


Fig. 9 The cascaded splitting ratios obtained from the experimental work at different radial positions when the bifurcation angle is 85° ($R_g = 0.3$ mm in both cases)

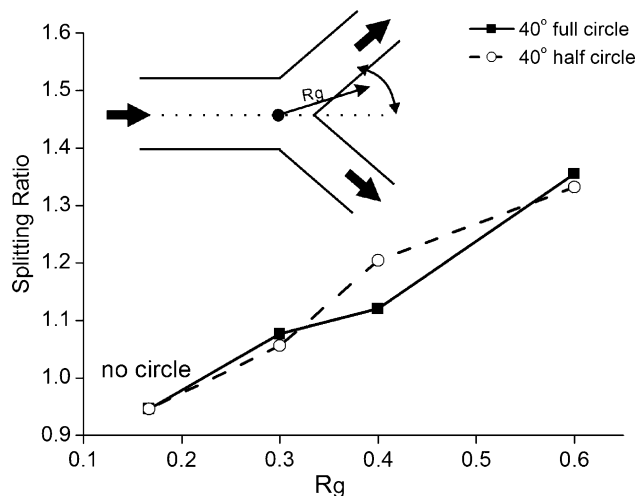


Fig. 10 The effects of different circle sizes on the splitting ratios when the bifurcation angle is 40°. $R_g = 0.3, 0.4$, and 0.6 mm for the full-circle and half-circle structures

4.2.2 Effects of circle dimensions and bifurcation angles

The buffer region will hold the stream lines and provide better splitting ratios during ELISA CD rotation. Effects of circle dimension (i.e., radius) were also of interest in the experimental study. Figure 10 shows the effects of circle radii 0.3, 0.4, and 0.6 mm in both half-circle and full-circle structures under bifurcation angle of 40°. The splitting ratios monotonically decrease to the value below 1. The no-circle design therefore can produce an unbalance splitting ratio. The full-circle and half-circle designs have less impact on the smaller bifurcation angle as we observed in Fig. 10. As we increase the bifurcation angle, the full-circle design produces larger splitting ratios as shown in Fig. 11. In practice, a smaller bifurcation angle is not a preferred

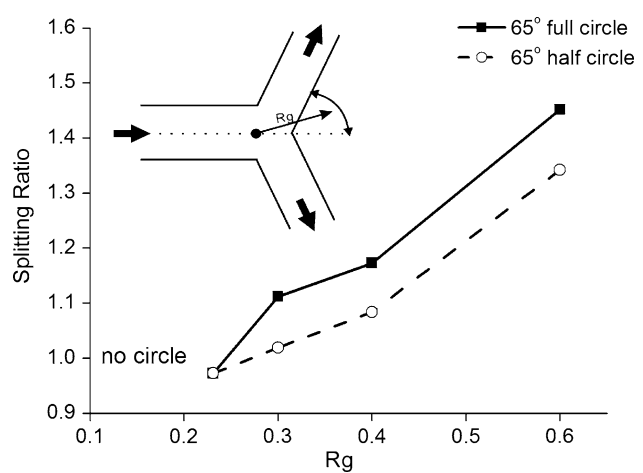


Fig. 11 The effects of different circle sizes on the splitting ratios when the bifurcation angle is 65°. $R_g = 0.3, 0.4$, and 0.6 mm for the full-circle and half-circle structures

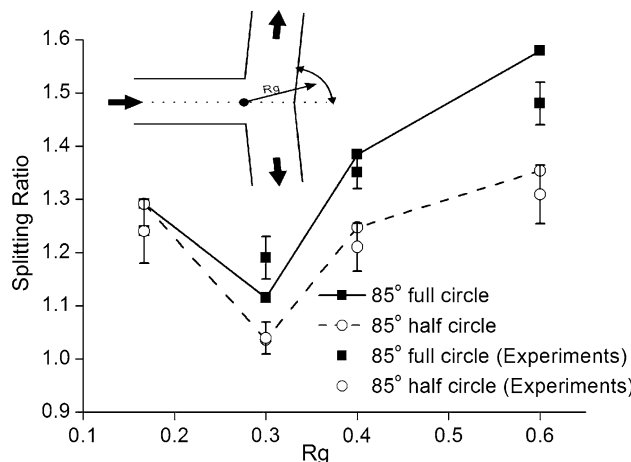


Fig. 12 The effects of different circle sizes on the splitting ratios when the bifurcation angle is 85°. $R_g = 0.3$, 0.4, and 0.6 mm for the full-circle and half-circle structures. Both simulated and experimental results are presented

design since the separation distance is limited and there is no spacing for the cascaded splitters along the channel. The larger bifurcation angle, such as 85° used in our experimental work, has shown enough space for the cascaded splitters in a CD (Lu et al. 2007). The 3D simulation results of 85° bifurcation angle are shown in Fig. 12. The splitting ratios of full-circles with radii 0.3, 0.4, and 0.6 mm were 1.12, 1.38, and 1.55, respectively, in simulated results. As we remove the radius, the simulated splitting ratio jumps to 1.29 due to the flow movement pushed by Coriolis force. The experimental measurements show a similar trend in these radii changes. The deviation between simulated and experimental results may result from channel surface machining quality (such as contact angle and roughness) as we outline in the following section.

4.2.3 Effects of surface roughness

In order to simplify the mathematical model arising from the complex surface conditions of the interior flow

channels in the splitter, we ignored surface conditions, such as roughness and contact angles in the numerical computations. However, these factors were included in the experiment and some preliminary results are included in this study. The CNC machining PMMA surface was measured to be $R_a = 0.34\text{--}0.36 \mu\text{m}$, which is slightly higher than the injected molded CD ELISA ($R_a = 0.2\text{--}0.3 \mu\text{m}$). Due to the nature of machining methods, the CNC-machined channel is considered to have a higher roughness value than the molded article. To eliminate the effects caused by surface roughness in the experiment, we carefully machined the PMMA and controlled the channel surface to within $R_a = 0.34\text{--}0.36 \mu\text{m}$. After the flow passes the splitter region, we change the roughness to $R_a = 0.41\text{--}0.43 \mu\text{m}$ (case #1) and $R_a = 0.55\text{--}0.96 \mu\text{m}$ (case #2) (see Fig. 13a for R_a distributions in the channel surfaces). Here, we repeated our experiments and measured the splitting ratios at 1000 rpm with a half-circle design ($R_g = 0.3 \text{ mm}$ in both cases). Figure 13b shows the splitting ratios for both cases. Case #1 has a surface roughness value of $R_a = 0.4\text{--}0.43 \mu\text{m}$, whereas case #2 has $R_a = 0.55\text{--}0.96 \mu\text{m}$. The splitting ratio remains equivalent in case #1. However, this even slitting is not observed in case #2. This indicates that the roughness variation from $R_a = 0.34\text{--}0.43 \mu\text{m}$ (i.e., the higher-lower ranges between $R_a = 0.41\text{--}0.43 \mu\text{m}$ and $R_a = 0.34\text{--}0.36 \mu\text{m}$) can still hold optimum splitting ratio under the current design. If two bifurcations have large differences in roughness (such as $\Delta R_a = 0.41$ in this case), the splitting ratio will be greatly affected as shown in Fig. 13b.

4.2.4 Demonstration on the CD-ELISA experiment

We integrated oxygen plasma with TR-catalyzed protein A technique to immobilize antibodies onto a PMMA-based ELISA microchip for the detection of interferon- γ (IFN- γ), a pluripotent cytokine that exert a broad spectrum of biological activities ranging from the modulation of immune responses to the regulation of cell proliferation and

Fig. 13 **a** The surface roughness was measured using an interferometer on the oval shaped area. **b** The effects of different channel roughness on the splitting ratio. The roughness ratios on the x-axis label indicated the measurements of two bifurcations. There are two cases studied here: case #1 $R_a = 0.4\text{--}0.43 \mu\text{m}$ and case #2 $R_a = 0.55\text{--}0.96 \mu\text{m}$

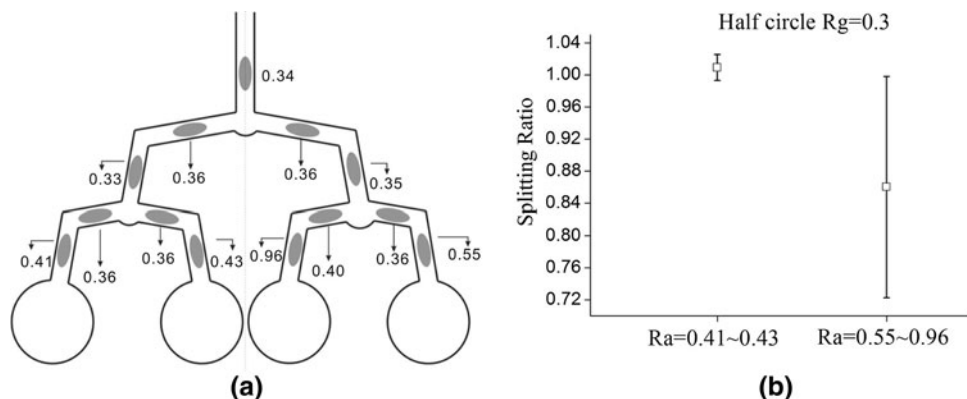


Table 3 Materials and reagents used in the CD-ELISA experiment

PEI	0.2% (w/v) in ddH ₂ O, 10 μl
Protein A:tyrosinase	5:1 in PBS, 10 μl
Capture antibody	1 μg/ml in PBS, 10 μl
Standards	1000 pg/ml, 500 pg/ml in Quench, 10 μl
Detection antibody	1 μg/ml in PBS, 10 μl
Streptavidin-HRP	1:4000 in PBS, 10 μl
Substrate solution	HPPA, 10 μl

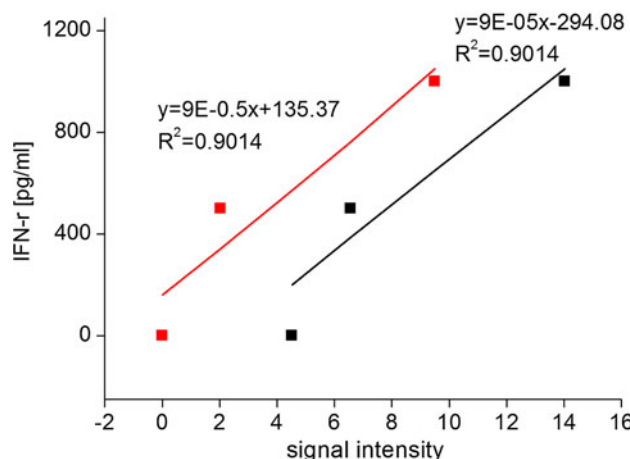


Fig. 14 The standard curve for human IFN- γ used ELISA assay to measure different concentrations in a CD disk then use LC-FL to detect the signal intensity at Ex320, Em405. The plots show good correlation between two detection holes (the background signal has been removed in one set) (measurements provided from Ye and Shi's lab at NFU, Taiwan)

apoptosis. The experimental procedure was listed in Table 3. Such cytokine concentration is commonly detected by ELISA. Prior to protein A immobilization, oxygen plasma, an widely used tool for functionalizing the surface chemistry and changing the surface morphology, was used to activate the inert PMMA followed by PEI coating.

Figure 1a shows a single assay on the 12-set CD-ELISA disk. The primary antibody was preimmobilized at the detection area. The mixture of antigen and second antibody was loaded in reservoirs 1 and 1A. Reservoirs 2 and 4 were used for washing solution. Reservoirs 3 and 5 were used for conjugate and substrate, respectively. A detail experimental work and operation procedure can be found in He et al. (2009). The standard curve for human IFN- γ was used ELISA assay to measure different concentrations in PMMA microchannels modified with protein A immobilization through TR-catalyzed reaction CD disk then used liquid chromatography fluorescence detector (LC-FL) to detect the signal intensity at Ex320, Em405. The result was shown in Fig. 14 with good linear correlations between concentration and signal intensity in two detection areas.

5 Conclusions

CD-ELISA is used to perform ELISA-based processes on a CD microfluidic platform. This concept allows us to utilize its unique microfluidic function, i.e., flow sequencing, to replace the stepwise procedures carried out in conventional ELISA processes. Major microfluidic components in CD-ELISA include sample loading, propulsion of fluids, use of valves, fluid mixing, sample splitting, and washing. The main challenge in making a microfluidic ELISA splitter is to create even splitting during operation. Uneven splitting is caused by a Coriolis force. In this study, we have proposed a buffer-structure splitter design and it has experimentally demonstrated even splitting. The major results are summarized below.

1. The theoretical derivation included in this study can serve as a preliminary design tool for a microfluidic device, such as splitter geometry and channel layout.
2. The half-circle splitter design is considered to be a buffer zone and it is experimentally verified to provide an even splitting function during CD-ELISA operation, where a Coriolis force is present. The half-circle structure provides better splitting ratio when compared with the full-circle structure.
3. The surface quality of the microfluidic channel can affect the splitting ratio. With current half-circle design, a roughness of $R_a = 0.34\text{--}0.43 \mu\text{m}$ still displays an optimum splitting ratio.

Acknowledgments This study was partially funded by the Taiwan Ministry of Education under the superior advance program. The authors would like to thank Dr. James Lee from Ohio State University for all of his help. The authors would also like to thank Dr. Yi-Ling Ye and Dr. L-S Shi at National Formosa University for the ELISA experimental work using our provided CDs.

References

- Anderson NG (1969) Computer interfaced fast analyzers. *Science* 166:317–324
- Brenner T, Glatzel T, Zengerle R, Ducre'e J (2005) Frequency-dependent transversal flow control in centrifugal microfluidics. *Lab Chip* 5:146–150
- Bonte M, Bonte-Leconte O, Rambaux-Hequet (1977) Fast immunochemical assay of proteins with Gemsaec centrifugal analyser. Application to serum transferrin and IgA assay. *J Ann Biol Clin* 35(3):227–235
- He H, Yuan Y, Wang W, Chiou N-R, Epstein AJ, Lee LJ (2009) Design and testing of a microfluidic biochip for cytokine enzyme-linked immunosorbent assay. *Biomicrofluidics* 3:022401
- Henry V, Deutsch J, Gifford L (1978) Enzyme immunoassay of theophylline with a centrifugal analyzer, and comparison with an ultraviolet method. *Clin Chem* 24(3):514
- Klumpp T (1977) Enzymic determination of serum antitrypsin activity by centrifugal analysis. *Ann Biol Clin* 35(3):221–226

- Lin S, Chen RS (2008) Parametric study on the burst frequencies of fishbone capillary valve used in the microfluidic CD ELISA. In: The 15th computational fluid dynamics conference, Taipei, Taiwan, ROC, 7–10 August
- Lu C, Xie Y, Yang YM, Cheng MC, Koh CG, Bai YL, Lee J, Juang YJ (2007) New valve and bonding designs for microfluidic biochips containing proteins. *Anal Chem* 79:994–1001
- Scott CD, Burtis CA (1973) A miniature fast analyzer system. *Anal Chem* 45(3):327A–339A
- Silva G, Leal N, Semiao V (2009) Critical pressure for capillary valves in a Lab-on-a-Disk: CFD and flow visualization. *Comput Struct.* doi:[10.1016/j.compstruc.2009.01.014](https://doi.org/10.1016/j.compstruc.2009.01.014)